Superstructure Control in the Crystal Growth and Ordering of Urea Inclusion Compounds

M. D. Hollingsworth,* M. E. Brown, A. C. Hillier,†
B. D. Santarsiero, J. D. Chaney

A template-directed mechanism of crystal growth is demonstrated for urea inclusion compounds (UICs). For UICs containing *n*-alkanone or α+1,ω−1-alkanedione guests, x-ray diffraction revealed superstructure relations between host and guest repeats along the channel axis for guests containing 8 to 14 carbons. For a favorable structural match between host and guest, UICs typically grow as flat hexagonal plates, and atomic force microscopy of {001} surfaces revealed molecularly smooth terraces differing in height by multiples of the guest repeat. If the match is poor, protrusion of guests from the {001} surfaces nucleates growth along the channel axis to form hexagonal needles.

Although attachment energy models (*1*) are useful tools for predicting the morphology of one-component molecular crystals under sublimation conditions, the dynamic role of the solvent and the kinetic properties of attachment and inclusion of solute have received significant attention recently (*2*). Much less attention has been paid to the molecular mechanisms of crystal growth of multicomponent crystals such as inclusion compounds, charge-transfer salts, and co-crystals (*3*). Here we demonstrate the existence of a template-directed mechanism in the crystal growth of channel inclusion compounds of urea. This mechanism embodies the terrace-ledge-kink model for surface growth (*4*), but it includes as its initiation step a dynamic and topographical component that is ultimately controlled by the superstructural relations between the urea host and its aliphatic guest. Although such superstructures are rarely observed in the x-ray diffraction (XRD) patterns of urea inclusion compounds (UICs), their role in the crystal growth process was revealed by a combination of XRD, atomic force microscopy (AFM), and crystal habit studies for a series of *n*-alkanone and bis(methyl ketone) UICs. The processes demonstrated here should apply to a variety of supramolecular assembly processes, including the formation of biological structures and zeolites.

Incommensurate UICs. In most UICs, urea molecules are connected by hydrogen bonds to form helical ribbons, which repeat every six urea molecules (11.0 Å) to form a series of linear, hexagonal tunnels that contain straight-chain hydrocarbons and substituted analogs (Fig. 1A) (*5*). The channel centers of this honeycomb network are separated by ~8.2 Å. Because the channel walls are smooth and rigid and have internal diameters that are somewhat larger than the van der Waals envelope of a polymethylene chain, guest molecules are held loosely and typically undergo substantial motions, including translations (*6, 7*) and diffusive motions or jumps about the channel axis. With few exceptions (*8–11*), UICs are incommensurate; that is, there are no reasonably small integers m and n for which $nc_h = mc_g$, where c_h and c_g are the typical host and guest repeat distances along the channel axis (Fig. 1B).

For these incommensurate UICs, solid-state nuclear magnetic resonance (NMR) confirms that the guests reside in a multitude of roughly equivalent environments (*12*) and pack within van der Waals contact along the channel axis. For a large fraction of UICs studied to date, XRD at 20°C shows that the guest molecules are uniformly spaced along each channel but have no spatial correlations between channels [one-dimensional (1D) ordering]. Certain classes of guests, however, show interchannel (3D) ordering (*13*). These guests include certain α,ω-disubstituted alkanes [in which the offset between guests in adjacent channels (Δ_g) (Fig. 1B) is $c_g/3$], several long-chain diacyl peroxides (in which Δ_g = 4.6 Å), and several symmetric anhydrides (for which Δ_g = 0 Å). In almost all cases, XRD indicates that these crystals are incommensurate UICs with hexagonal metric symmetry.

Ordering of guests in alkanone/UICs. Here we report that a wide variety of long-chain alkanones and alkanedione UICs exhibit pronounced interchannel guest ordering with Δ_g = 0 Å. In the channel-axis oscillation experiment, the XRD pattern comprises layer lines characterizing the repeats of the host and guest along the channel. With the exception of (*hk*0), these layer

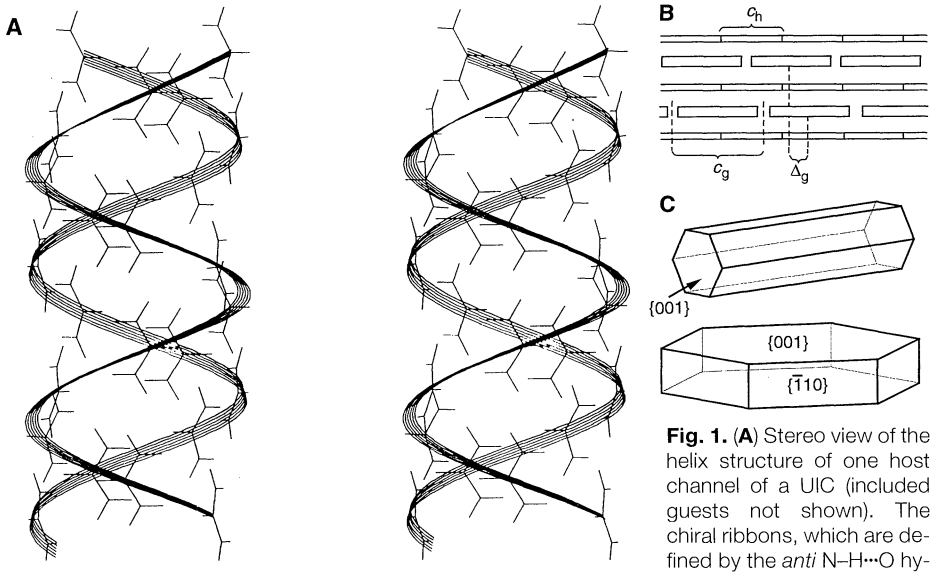

Fig. 1. (**A**) Stereo view of the helix structure of one host channel of a UIC (included guests not shown). The chiral ribbons, which are defined by the *anti* N–H···O hydrogen bonds, run antiparallel to each other along the *c* axis and are linked by *syn* N–H···O hydrogen bonds. These hexagonal channels are linked by their edges to form a solid-state honeycomb structure [coordinates from (*14*)]. (**B**) A 2D view of an incommensurate UIC indicating definitions of c_g, c_h, and Δ_g. For commensurate systems, c'_g denotes the average molecular repeat distance for the guest and c'_h denotes the 11.0 Å repeat for six urea molecules (*17*). (**C**) Hexagonal needle and plate habits of UICs. For UICs in which interchannel guest ordering is strong and Δ_g = 0 Å, the latter is favored (Table 1). All of the bis(methyl ketone)/UICs we report exhibit the flat-plate morphology.

M. D. Hollingsworth, M. E. Brown, and J. D. Chaney are in the Department of Chemistry, Indiana University, Bloomington, IN 47405, USA. A. C. Hillier is in the Department of Chemical Engineering and Materials Science, University of Minnesota, Minneapolis, MN 55455, USA. B. D. Santarsiero is in the Department of Chemistry, University of California, Berkeley, CA 94720–1460, USA.

*To whom correspondence should be addressed.
†Present address: Department of Chemical Engineering, University of Virginia, Charlottesville, VA 22903, USA.

lines can be classified as either host (h) or guest (g), with the understanding that each pattern contains contributions from the other substructure (*14*). At low 2θ angles, between the h layer lines [such as $(hk1)_h$ and $(hk2)_h$] that characterize the 11.0 Å repeat of the urea helix, one typically observes layer lines [$(hk1)_g$, $(hk2)_g$] that are dominated by guest diffraction. Depending on the guest length and substitution pattern, these g layer lines reveal different degrees of guest ordering. If guests ordered only within individual channels (1D ordering), the g layer lines comprise diffuse bands without discernible maxima (Fig. 2A). If significant positional correlations existed between guests in adjacent channels (3D ordering), however, the g layer lines comprised discrete reflections.

Almost all of the alkanone/UICs that we have studied (Table 1) exhibit interchannel ordering of guests with $\Delta_g = 0$ Å (instead of 1D ordering) and display a distinctive habit that could be directly linked to this ordering. From methanol solutions, alkanone/UICs that exhibited pronounced 3D ordering of guests (for example, 2-undecanone/urea) showed a strong tendency to grow as flat {001} hexagonal plates; if the guests exhibited only 1D ordering (as in 2-decanone/urea), however, the crystals grew as long hexagonal needles, which is the typical habit observed for UICs (Fig. 1C) (*15*). With only one clear exception (*9*), the guest repeat lengths from XRD measurements suggested that the alkanone/UICs that we have studied are incommensurate systems.

These observations present a difficult quandary. If these UICs are truly incommensurate, why do the guests exhibit such well-defined interchannel ordering? Furthermore, how does the interchannel ordering of guests control the crystal habit? Although mechanisms involving interchannel dipole-dipole interactions between guest molecules were evaluated (*16*), our XRD studies of a homologous series of bis(methyl ketone)/UICs have revealed the predominant importance of host-guest interactions that control the guest ordering and crystal growth of the alkanone/UICs. In the diketone/urea series, addition of a second carbonyl dramatically reduced the thermal diffuse scattering observed in the g XRD patterns and in doing so revealed the commensurate relations between the hosts and guests.

For each of the bis(methyl ketone)/UICs from C_8 to C_{14}, the XRD pattern showed that $\Delta_g = 0$ and that a commensurate relation exists for the host and guest repeat distances (Fig. 3). Instead of observing dis-

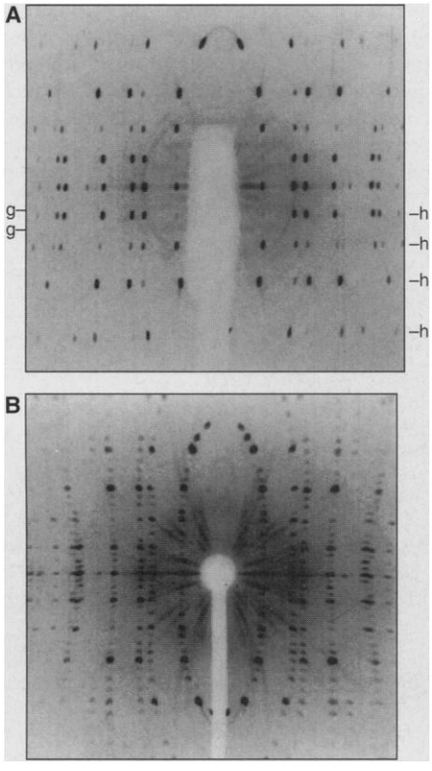

Fig. 2. Channel-axis oscillation photographs of (**A**) 2-decanone/urea and (**B**) 2,9-decanedione/urea. In (A), the diffuse bands in the horizontal g layer lines are indicative of 1D ordering of guests (see markers). In (B), the intense superstructure pattern characterizes the commensurate relation of $3c'_g = 4c'_h$. [The (*hk*0) layer is in the center of each photograph.]

Table 1. Guest repeats, ordering, and representative crystal habits of selected alkanone/UIC crystals in order of decreasing aspect ratio. All were grown by cooling solutions of the guest (approximately 1.0 g, ≥99% purity) in 20 ml of 1.8 M urea in methanol from 45° to 20°C (to 5°C for short-chain guests) at ~2°C per hour. Numbers in parentheses are standard deviations in the last digit or digits. Aspect ratios (crystal length along channel axis/largest dimension of {001} face) were measured for an average of 74 randomly selected crystals from a given batch. The sequence of guest ordering patterns (1D and 3D) represents an estimate of their prominence in the pattern.

Guest	c_g (Å)	Habit	Mean aspect ratio	Guest ordering
2-Decanone	15.1(1)*	Long needles	11.1(45)	1D only
2-Nonanone	13.7(1)*	Long needles (poorly formed)	N/A	1D only
3-Undecanone	16.25(10)†	Long, thick needles	9.1(37)	1D + weak 3D
4-Undecanone	16.24(10)†	Poorly formed needles	5.9(32)	3D + 1D
5-Nonanone	13.8(1)*†	Chunky needles and thick plates	3.8(22)	3D + weak 1D
5-Decanone	15.1(1)†	Chunky needles and thick plates	3.1(21)	3D + 1D
6-Tridecanone	18.7(1)†	Thick plates	1.9(10)	3D + 1D
2-Dodecanone	17.46(2)‡	Thick plates and chunky needles	1.4(10)	3D + 1D
3-Decanone	15.2(1)†	Thick plates	1.2(12)	3D + 1D
5-Undecanone	16.55(2)§	Thick plates	1.0(9)	3D + 1D
7-Tridecanone	18.74(6)‡	Thick plates	0.9(6)	3D + 1D
6-Undecanone	16.16(5)§	Thin plates	0.32(31)	3D + weak 1D
2-Undecanone	16.27(7)§	Thin plates	0.30(12)	3D + weak 1D
2-Tridecanone	18.85(3)‡	Extremely thin plates	0.08(3)	3D + 1D

*From oscillation photograph; errors are estimated visually. †From the (001) g reflection from powder XRD. ‡From least-squares refinement of several powder XRD maxima. §From single-crystal diffractometry. Although this crystal has hexagonal metric symmetry, diffractometry reveals weak reflections for twinned orthorhombic cells rotated by 60° relative to each other. [For a related case, see (*9*).]

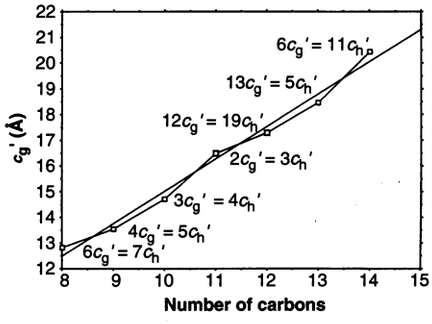

Fig. 3. Repeat distance of guest along channel axis (c'_g) versus chain length for bis(methyl ketone)/UICs, showing commensurate relations between guest and host (c'_h) repeat lengths (*17*). The straight line depicts the best fit through the points shown. Five of the guests can share screw axes with the helical host structure (C_8, 6_1; C_{10}, 3_1; C_{11}, 2_1; C_{13}, 3_1; and C_{14}, 6_1), whereas two others (C_9 and C_{12}) require more than one type of host-guest interaction in the asymmetric unit of the supercell and show poorer structural matches between host and guest (*28*). For C_{12}, this supercell gives a molecular relation between two guest molecules and 19 host molecules. Values of c'_g for different chain lengths are as follows (in angstroms; numbers in parentheses are standard deviations in the last digit or digits): C_8, 12.84(2); C_9, 13.57(5); C_{10}, 14.73(1); C_{11}, 16.491(3); C_{12}, 17.31(3); C_{13}, 18.47(1); and C_{14}, 20.24(1).

crete reflections or diffuse bands corresponding to the periodicities (c_h and c_g) of the ordinary host and guest substructures (as in most UICs), we observed discrete scattering on additional layer lines, as shown in the oscillation photograph of 2,9-decanedione/urea (Fig. 2B). This UIC is thus a commensurate phase for which $3c'_g = 4c'_h$ (*17*). The unit cell has a length of 44.0 Å (4 × 11.0 Å and 3 × 14.7 Å), with three guest molecules related along the channel axis by a three-fold screw axis. Similarly, for 2,7-octanedione/urea, there are six guest molecules for every seven turns of the urea helix, and the resultant unit cell repeat along the channel axis is 77.0 Å. In the five UICs for which the metric properties of the superstructure allow hosts and guests to share 2_1, 3_1 or 6_1 screw axes, the observed "superstructure pattern" was quite strong. For the other two systems, there was no simple structural match between host and guest, and the superstructure patterns were much weaker.

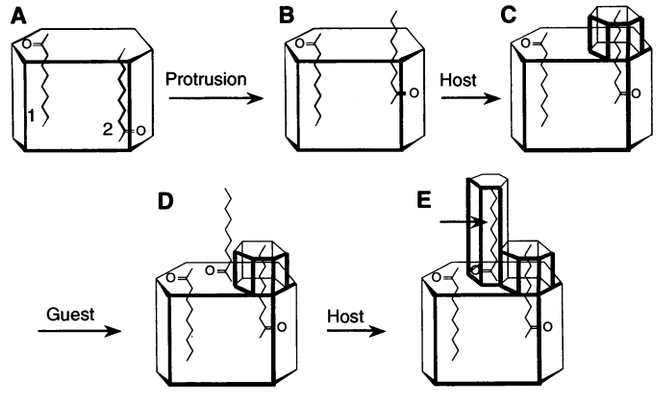

Fig. 4. Template-directed mechanism for nucleation and crystal growth along channel axis of UICs. (**A**) Starting position. In this model, guest 2 protrudes (**B**) from its starting position at Δ_g = 0 Å relative to guest 1 before urea molecules add to this surface site (**C**) to form a binding site to which a third guest can add (**D**). Guest-directed addition of urea forms a terrace (**E**) that is one guest molecule high. Successive addition of guest and host to the {$\bar{1}$10} faces of this terrace (arrow) build the terrace rapidly in two dimensions. In crystals for which a favorable superstructural match exists between host and guest, the initial protrusion is inhibited, and lateral growth is preferred. In those same crystals, stage E is probably followed by recession of guest 2 (to Δ_g = 0 Å) and dissolution of the metastable binding site to give a flat {001} surface. For crystals in which $\Delta_g \neq 0$ Å, the roughened surface topography promotes crystal growth along the channel axis to form {001} needles or prisms exhibiting higher index facets.

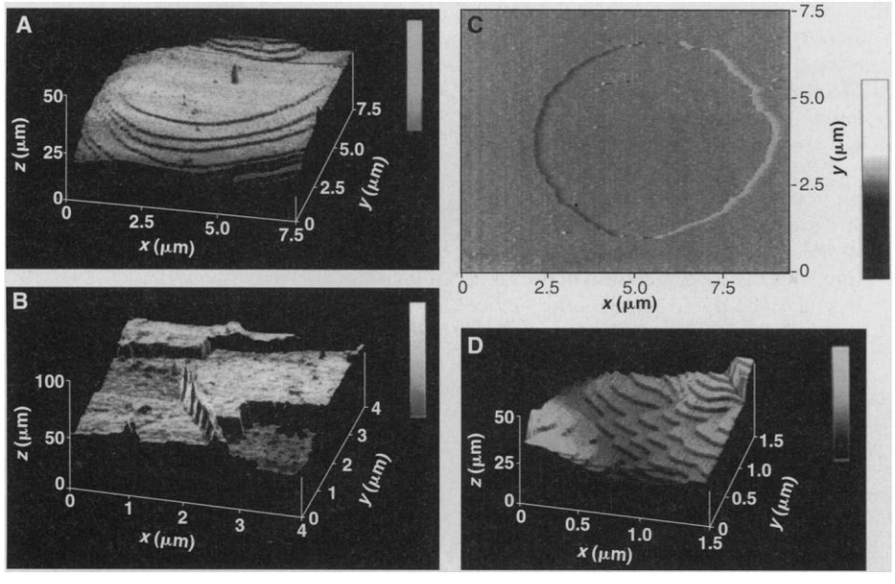

Fig. 5. AFM images of the {001} faces of alkanone and alkanedione/UICs recorded with a Digital Nanoscope III in tapping mode. (**A**) 2,9-Decanedione/urea ($3c'_g = 4c'_h$) in air. The average step height for 14 different ledges on this crystal was 15.7(11) Å. The shades of the scale bar span 25 nm. (**B**) 2,11-Dodecanedione/urea ($12c'_g = 19c'_h$) in air. Note the increased scale in the *z* direction and the absence of molecularly smooth ledges. Scale bar: 50 nm. (**C**) 2,10-Undecanedione/urea ($2c'_g = 3c'_h$) during dissolution under a nearly saturated solution of urea:guest (9:1) in ~10:1 *tert*-butyl alcohol: methanol. Scale bar: 17.4 nm. (**D**) 8-Pentadecanone/urea in air. Each ledge is ~20 Å high. This substance and 2,14-pentadecanedione/urea exhibit 3D guest ordering with Δ_g = 0 Å, but the weak nature of the superstructure reflections prevents an unambiguous assignment. Scale bar: 25 nm.

Because of compensating changes in bond lengths and bond angles, the lengths of the corresponding alkane, alkanone, and alkanedione molecules are almost identical. Indeed, the commensurate relations observed for the alkanedione/UICs can be used to understand the guest ordering observed for alkanone/UICs. Although the superstructure patterns are either weak or absent for the alkanone/UICs under normal x-ray exposure conditions, it is almost always possible to observe these superstructure patterns after long x-ray exposure at room temperature, especially with stationary crystals (the Laue method) (*18*). In cases such as 2-decanone/urea, in which the guests exhibited only 1D ordering at 292 K, cooling the crystal to 188 K revealed essentially the same superstructure pattern observed for 2,9-decanedione/urea ($3c'_g = 4c'_g$). In all cases that we have studied thus far, the essential features of the superstructure patterns observed for the alkanone/UIC are virtually the same as those observed for the alkanedione/UIC with the same guest chain length, showing that the interchannel ordering of guests with Δ_g = 0 Å arises primarily from their interactions with the host (*19*).

Template-directed growth. The superstructural relations between host and guest suggest a template-directed mechanism for the crystal growth of UICs, in which needle-like growth along the channel axis is catalyzed by translation or protrusion of the guest molecules from the {001} surfaces (Fig. 4B). Formation of new ledges begins when the host wraps around exposed guest molecules (Fig. 4C). Lateral growth can then propagate through the same sort of template effect (Fig. 4, D and E), in which guest molecules bind to ledge and kink sites and are then surrounded by urea molecules. Accordingly, incommensurate UICs should grow as hexagonal needles, as should those for which the offset between guests in adjacent channels is nonzero or the interchannel ordering is weak (*20*). However, for UICs with well-defined superstructures in which Δ_g = 0 Å, the {001} faces may be capped off (Fig. 4A) and the surface energy lowered. New material is therefore added to the sides of the ledges, and the formation of new ledges is minimized because host-guest interactions inhibit longitudinal motion of the guests and because 2D nucleation, rather than direct attachment, is required for growth normal to the {001} plane.

Atomic force microscopy in air of bis(methyl ketone)/UICs provided strong evidence for this template mechanism of crystal growth. For each type of bis(methyl ketone)/urea crystal exhibiting a favorable superstructure, we found molecularly smooth ledg-

es on the {001} faces (as in Fig. 5A). As predicted by the template mechanism, the vast majority of the ledge heights were integral multiples of the guest repeat, and short steps corresponding to the addition of small numbers of urea molecules to the {001} surface were rare. In contrast, crystals of 5-nonanone/urea, 2,8-nonanedione/urea, and 2,11-dodecanedione/urea gave extremely rough {001} surfaces with few molecularly smooth ledges, as expected for the poor matches between the host and guest substructures (Fig. 5B). These results are consistent with the proposed mechanism of crystal growth, as are in situ dissolution experiments with 2,10-undecanedione/urea (c'_g = 16.5 Å), in which we observed the growth of a molecularly flat oval pit several micrometers in diameter and 17 Å deep (Fig. 5C). Longer chain guests such as 8-pentadecanone can also form UICs with smooth {001} terraces (Fig. 5D), even though the superstructure patterns are weak; here, the increased host-guest interactions for longer guests may inhibit longitudinal motion and protrusion of guests from the {001} terraces, which are again typically offset by multiples of c'_g.

Hydrogen bond interactions. The crystal structure of 2,9-decanedione/urea reveals a detailed picture of the profound way that host-guest hydrogen bonding (H bonding) controls the interchannel ordering and crystal growth in this series of inclusion compounds. Just as in 2,10-undecanedione/urea (*11*), guest molecules in 2,9-decanedione/urea are tethered by urea molecules that turn about their twofold axes so that their *syn* hydrogens make H bonds with guest carbonyls in adjacent channels (*21*). In its extended form (with its C=O bonds antiparallel), 2,9-decanedione should have an average length of 15.1 Å (the c_g observed in 2-decanone/urea), but this length is 0.4 Å longer than the commensurate repeat. To lock into the commensurate structure, this guest shortens itself by coiling so that its C=O groups form H bonds to urea molecules on two adjacent walls of the channel (Fig. 6). This severe twisting of 2,9-decanedione explains why 2-decanone/urea forms hexagonal needles that exhibit only 1D ordering of guests at 292 K. Without carbonyl tethers at its two ends, 2-decanone cannot form enough H bonds to compensate for the excess torsional energy of twisting, and it therefore cannot easily form a commensurate structure. The guest molecules that dangle from the {001} surface therefore provide a multitude of nucleation sites for new growth along the channel axis, and needle-like crystals form (*22*).

Competing pathways. The kinetic mechanism presented in this article competes with pathways that favor the thermodynamic (plate) form. For example, when we incubated hexagonal needles from a first crop of 2-decanone/urea at 295 K for 5.7 months in the methanol solution from which they were grown, they converted slowly into thick plates [mean aspect ratio = 3.4 ± 2] by a solvent-mediated transformation (*23*). Other UICs that give needles, such as 5-nonanone/urea, showed similar solution incubation behavior. The conversion from needles to plates is probably related to slow dissolution of the metastable terraces (upper right of Fig. 4E); this process lowers the surface energy of the {001} face and allows lateral growth to compete with the kinetic processes that give rise to needle formation. Consistent with this notion is our observation that alkanone/UICs exhibiting intermediate or platelike habits in methanol (such as 2-dodecanone/urea) form long needles when grown from isobutyl alcohol (*24*). In this solvent, the low solubility of urea inhibits dissolution of the metastable terraces and favors the kinetic process (*25*). In the case of 2-decanone/urea grown from methanol, the same weak binding to the host that favors protrusion of guest molecules in the nucleation step (Fig. 4B) probably disfavors recession of the guest to Δ_g = 0 Å and the lowering of the surface energy of {001} that gives rise to plates (*26*). This slow transformation into plates at 295 K may arise from an unobserved bias (*27*) toward the commensurate structure in which Δ_g = 0 Å, as indicated by the diffraction pattern observed for 2-decanone/urea at 188 K. Such dynamic processes present a formidable challenge to chemists who try to control the shapes of crystals. Nevertheless, the phenomena revealed here provide a predictive framework for developing a clearer understanding of the crystal growth of inclusion compounds and other supramolecular assemblies.

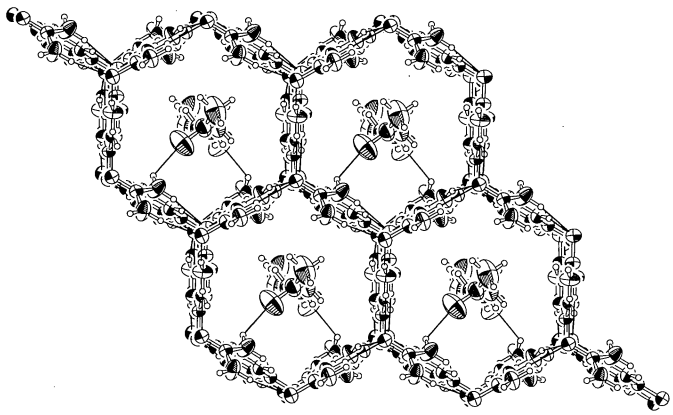

Fig. 6. ORTEP (*29*) view down the channel axis of 2,9-decanedione/urea (30% ellipsoids). One layer of guests is shown. Guest molecules coil so that their carbonyls make H bonds with ureas on adjacent channel walls. These same ureas tether guests with different *z* coordinates in adjacent channels. [$C_9H_{25}N_8O_5$: space group $P3_112$, z = 6, $a = b$ = 8.229(2) Å, c = 44.16(2) Å; R = 0.070 and R_w = 0.088 on the basis of full-matrix least-squares refinement of 2043 unique observations (intensities $I > 3\sigma(I)$).]

REFERENCES AND NOTES

1. Z. Berkovitch-Yellin, *J. Am. Chem. Soc.* **107**, 8239 (1985).
2. L. J. W. Shimon, M. Vaida, L. Addadi, M. Lahav, L. Leiserowitz, *ibid.* **112**, 6215 (1990).
3. B. Kahr and J. M. McBride, *Angew. Chem.* **104**, 1 (1992); M. Vaida *et al.*, *Science* **241**, 1475 (1988); A. Hillier, J. H. Schott, M. D. Ward, *Adv. Mater.* **7**, 409 (1995).
4. P. Bennema and G. H. Gilmer, in *Crystal Growth: An Introduction*, P. Hartman, Ed. (North-Holland, Amsterdam, 1973), pp. 263–327; P. Bennema and J. P. van der Eerden, in *Morphology of Crystals*, I. Sunagawa, Ed. (Terra, Tokyo, 1987), vol. A, pp. 1–75.
5. A. E. Smith, *Acta Crystallogr.* **5**, 224 (1952).
6. K. Fukao, H. Miyaji, K. Asai, *J. Chem. Phys.* **84**, 6360 (1986).
7. D. Schmicker, S. van Smaalen, J. L. de Boer, C. Haas, K. D. M. Harris, *Phys. Rev. Lett.* **74**, 734 (1995).
8. J. Otto, *Acta Crystallogr. B* **28**, 543 (1972).
9. M. D. Hollingsworth and C. R. Goss, *Mol. Cryst. Liq. Cryst.* **219**, 43 (1992).
10. M. D. Hollingsworth, B. D. Santarsiero, K. D. M. Harris, *Angew. Chem. Int. Ed. Engl.* **33**, 649 (1994).
11. M. E. Brown and M. D. Hollingsworth, *Nature* **376**, 323 (1995).
12. M. D. Hollingsworth and N. Cyr, *Mol. Cryst. Liq. Cryst.* **187**, 395 (1990).
13. K. D. M. Harris, S. P. Smart, M. D. Hollingsworth, *J. Chem. Soc. Faraday Trans.* **87**, 3423 (1991); K. D. M. Harris and M. D. Hollingsworth, *Proc. R. Soc. London Ser. A* **431**, 245 (1990); I. J. Shannon, N. M. Stainton, K. D. M. Harris, *J. Mater. Chem.* **3**, 1085 (1993).
14. K. D. M. Harris and J. M. Thomas, *J. Chem. Soc. Faraday Trans.* **86**, 2985 (1990).
15. Because each host-guest system gives rise to a unique set of structure factors, there is no single set of diffraction maxima that can be used to quantitatively compare the extent of interchannel guest molecule ordering in the different systems. Thus, a crude comparison of discrete and diffuse scattering from guests is given in Table 1. See N. Nicolaides, F. Laves, A. Niggli, *J. Am. Chem. Soc.* **78**, 6415 (1956).
16. For a discussion, see J. I. Lauritzen Jr., *J. Chem. Phys.* **28**, 118 (1958).
17. For incommensurate UICs, the typical host repeat along the channel axis (c_h) of 11.0 Å comprises six urea molecules. With commensurate UICs, c_h may be some other value (for example, 33.0 Å), so for these systems we use the terms c'_g and c'_h to denote the average molecular repeat distance for the guest and the 11.0 Å repeat for six urea molecules.
18. In several cases, superstructure reflections were observed for alkanone/UICs even though the measured guest repeat differed by somewhat more than 3σ from that predicted for the commensurate structure. With 2-undecanone/urea, for example, the g XRD pattern (which comprised relatively low-angle reflections) showed superstructure patterns for $2c'_g = 3c'_h$, but the guest repeat of 16.27(7) Å is less than the value of c'_g = 16.5 Å that is required for a commensurate structure. Although the source of this anomaly is not yet clear, the peak shifts suggest mixtures of

commensurate and incommensurate phases, which we observed in the powder XRD patterns of 2-undecanone/urea and 6-undecanone/urea. Other phenomena, such as dislocation effects on the positions of the Bragg maxima, have not yet been documented. See (6) and B. E. Warren, *Phys. Rev.* **59**, 693 (1941).
19. The much weaker 3D ordering (with $\Delta_g = 0$ Å) (6) of guests in linear alkane/UICs can be understood in terms of the same commensurate structures. [The guest repeats for alkanone/UICs (Table 1) are all within 0.1 Å of those reported for the analogous alkane/UICs. See H. U. Lenné, H. C. Mez, W. Schlenk Jr., *Justus Liebigs Ann. Chem.* **732**, 70 (1970).]
20. To our knowledge, only UICs containing guests with $\Delta_g = 0$ Å grow as {001} plates.
21. This common theme of bridging ureas is repeated in the crystal structure of 2,7-octanedione/urea. In this context, the pronounced interchannel ordering and extremely low aspect ratio for 2-tridecanone/urea (Table 1) can be seen as a special consequence of the commensurate relation ($3c'_g = 5c'_h$), the bridging by ureas of the terminal methyl ketone groups, and the long chain length of the guest (which inhibits guest protrusion).
22. In cases for which co-inclusion of guests is possible (such as mixtures of 2-undecanone and 6-undecanone), the 3D ordering of guests is diminished considerably, and needles are favored.
23. By solid-state NMR (12) and XRD, which probe intra- and interchannel ordering of guests, the needles and plates are structurally indistinguishable.
24. Mean aspect ratios for 2-dodecanone/urea and 2-undecanone/urea grown from isobutyl alcohol were 6 ± 2 and 13 ± 7, respectively. See (2) for an alternative role of solvent molecules.
25. In conjunction with this solvent dependence and (22), we note that the most dramatic example of habit modification we have observed occurred with mixed UICs of 1,10-dichlorodecane and 1,10-dicyanodecane grown from a 7:1 mixture of the guests and urea in isobutyl alcohol; the aspect ratios for these crystals were remarkably high and ranged from 500 to 2500.
26. The delicate nature of the {001} surfaces of 2-decanone/urea crystals resulted in continual etching during imaging, which prevented an accurate picture of the surface topography.
27. H. C. Chang, R. Popovitz-Biro, M. Lahav, L. Leiserowitz, *J. Am. Chem. Soc.* **104**, 614 (1982).
28. We have not yet determined the crystal structures of 2,12-tridecanedione/urea or 2,13-tetradecanedione/urea, so the presence of true crystallographic threefold or sixfold screw axes for these systems is still in question. For C_9 and C_{12} diketones, the metric properties of the diffraction patterns do not allow us to exclude alternative supercells with $9c'_g = 11c'_h$ (C_9) and $7c'_g = 11c'_h$ (C_{12}), but the oscillation photographs strongly favor the commensurate relations.
29. C. K. Johnson, *Rep. ORNL-3794* (Oak Ridge National Laboratory, Oak Ridge, TN, 1965).
30. We thank C. R. Goss, C. J. Nichols, M. D. Ward, A. E. Aliev, and K. D. M. Harris for their help with this work, and J. M. McBride for critical comments on the manuscript. This work was supported by the National Science and Engineering Research Council (Canada), the Petroleum Research Fund (administered by the American Chemical Society), the National Science Foundation (CHE-9423726), and the Alfred P. Sloan Foundation (fellowship to M.D.H.).

20 March 1996; accepted 3 July 1996

Mantle Viscosity and Ice-Age Ice Sheet Topography

W. Richard Peltier

Ice-age paleotopography and mantle viscosity can both be inferred from observations of Earth's response to the most recent deglaciation event of the current ice age. This procedure requires iterative application of a theoretical model of the global process of glacial isostatic adjustment. Results demonstrate that the iterative inversion procedure converges to a paleotopography that is extremely close to that from the ICE-4G model. The accompanying mantle viscosity profile is furthermore shown to reconcile the requirements of aspherical geoid anomalies related to the mantle convection process, thus resolving a fundamental issue concerning mantle rheology. The combined model also explains postglacial sea level histories for the east coast of the United States.

Global signatures of the glacial isostatic adjustment (GIA) process constrain both the viscosity of Earth's mantle and the weight of the extensive continental ice sheets that existed on Earth's surface at the last glacial maximum (LGM). The theory that has been developed to describe the GIA process (*1*, *2*) involves only these two unknowns, as the elastic structure of the spherically symmetric viscoelastic model Earth is assumed to be fixed to that of the seismologically constrained PREM (*3*). The problem of applying this theory to infer both deglaciation history and mantle viscosity on the basis of the observed response to deglaciation is nonlinear. Errors in our knowledge of either mantle viscosity or deglaciation history could, in principle, propagate into our inference of the other. The widely varying inferences of mantle viscosity that have appeared in recent literature could thus be a simple consequence of errors in the deglaciation history (*4*). Similarly, recently proposed models of the deglaciation history may be sensitive [for example, see (*5*)] to errors in the model of the radial variation of viscosity. Here I show that the iterative solution of this nonlinear problem converges to acceptably stable estimates of both mantle viscosity and deglaciation history and that the global model of GIA so constrained reconciles the observed postglacial relative sea level (rsl) history along the east coast of the North American continent for the first time.

Department of Physics, University of Toronto, Toronto, Ontario, Canada M5S 1A7.

As a starting point, I used the recently derived ICE-4G model of the history of deglaciation since the LGM (*1*). The variations in continental ice sheet thickness in this model were derived by inverting postglacial rsl histories through the use of a simple radial profile of mantle viscosity (referred to herein as M1), a three-layer model incorporating a lithosphere of thickness 120.6 km, an upper mantle and transition zone with a viscosity of 10^{21} Pa·s, and a lower mantle with a viscosity of 2×10^{21} Pa·s. In the family of simple three-layer parameterizations, this structure is the globally preferred structure (*6*, *7*) when the viscosity of the upper mantle and transition zone is fixed to the nominal value of 10^{21} Pa·s originally inferred by Haskell (*8*) on the basis of his analysis of the postglacial rebound of Fennoscandia. The ICE-4G deglaciation history differs significantly from that of CLIMAP (*9*) and is currently in use internationally as a lower boundary condition for a new generation of atmospheric general circulation model reconstructions of LGM climate. The issue of the validity of ICE-4G is therefore rather important. I investigate this matter by fixing the deglaciation history to ICE-4G and then refining the viscosity profile by applying well-established formal procedures. The refined viscosity profile (M2) was then used to recompute the response to deglaciation on which basis the ICE-4G model was originally inferred to demonstrate that full convergence of the solution is obtained with minor modification to ICE-4G.

Mantle viscosity from GIA. The formal procedure used to refine M1 was developed in a series of recent articles (*10*–*12*) in which the methodology of Bayesian inference (*13*) plays a critical role. The data (*11*, *12*) include the relaxation spectrum for the postglacial rebound of Fennoscandia (*14*) (see Fig. 3B for a plot of the spectrum) and site-specific relaxation times inferred from ^{14}C-dated emergence histories from six sites surrounding the Gulf of Bothnia, seven sites surrounding Hudson Bay, and 10 sites in the Canadian Arctic (Fig. 1, A and B). The formal inversion is also constrained by two anomalies of Earth's present rotational state (*11*): the ongoing wander of the planet's axis of rotation at the rate of ~0.95° per million years along the 76°W meridian and the so-called nontidal acceleration of the rate of axial rotation. This nontidal accel-